

CCi-YOLOv8n: Enhanced Fire Detection with CARAFE and Context-Guided Modules

*Note: Sub-titles are not captured in Xplore and should not be used

1st Kunwei Lv

School of Information Science and Technology

Tibet University

Lhasa, China

lkw872473172@163.com

Abstract—Fire incidents in urban and forested areas pose serious threats, underscoring the need for more effective detection technologies. To address these challenges, we present CCI-YOLOv8n, an enhanced YOLOv8 model with targeted improvements for detecting small fires and smoke. The model integrates the CARAFE up-sampling operator and a context-guided module to reduce information loss during up-sampling and down-sampling, thereby retaining richer feature representations. Additionally, an inverted residual mobile block enhanced C2f module captures small targets and fine smoke patterns, a critical improvement over the original model’s detection capacity. For validation, we introduce Web-Fire, a dataset curated for fire and smoke detection across diverse real-world scenarios. Experimental results indicate that CCI-YOLOv8n outperforms YOLOv8n in detection precision, confirming its effectiveness for robust fire detection tasks.

Index Terms—YOLOv8; Upsampling; Downsampling; Fire Detection

I. INTRODUCTION

Fire outbreaks, whether in urban centers or remote wilderness, can cause devastating losses due to delayed responses. Manual detection methods are slow and labor-intensive, requiring constant human oversight. In contrast, automatic fire detection enables real-time alerts that can curb fire spread and reduce casualties. Recent advancements include deep learning systems for wildfire detection [3, 23, 26], neural fuzzy systems for complex forest environments [2], and enhanced YOLOv8 models for urban fires [1, 24]. However, most models are environment-specific. Combining Himawari-8 satellite images with convolutional neural networks [4, 25] improved active fire detection accuracy, though real-time capability remains a challenge. A recent MobileNetV3-YOLOv4 model for embedded devices [5] offers faster detection but with some feature detail loss, affecting overall detection quality.

Due to the limitations of prior work, this study employs YOLOv8n as the baseline model, given its outstanding performance in the field of object detection. The original model utilizes a simplistic upsampling method in the neck, which

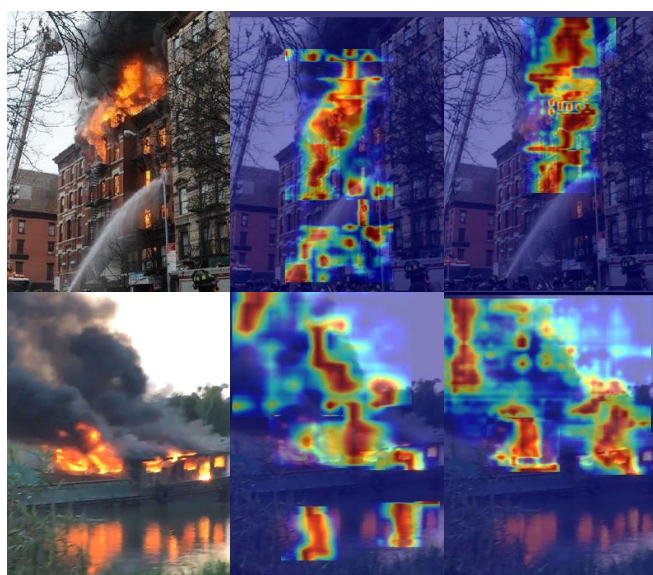


Fig. 1. The heatmap generated from the input image has poor detection results, where the red box represents the part that the heatmap does not detect, and the blue box represents the part that is falsely detected.

doubles the height (H) and width (W) while keeping the number of channels unchanged. In the backbone’s downsampling operations, standard convolution is used, which halves H and W and doubles the number of channels, thereby resulting in significant feature loss during sampling. Although the backbone’s C2f module enhances the original C3 module by incorporating a split operation and leveraging residual connections for optimization, the bottleneck component of the original model employs a relatively basic feature extraction approach, limiting its capacity for comprehensive feature extraction. Therefore, we propose an improved model, CCI-YOLOv8, to address these deficiencies. The proposed improvements aim to mitigate the feature loss issues during sampling and enhance feature extraction throughout the network, thereby improv-

Identify applicable funding agency here. If none, delete this.

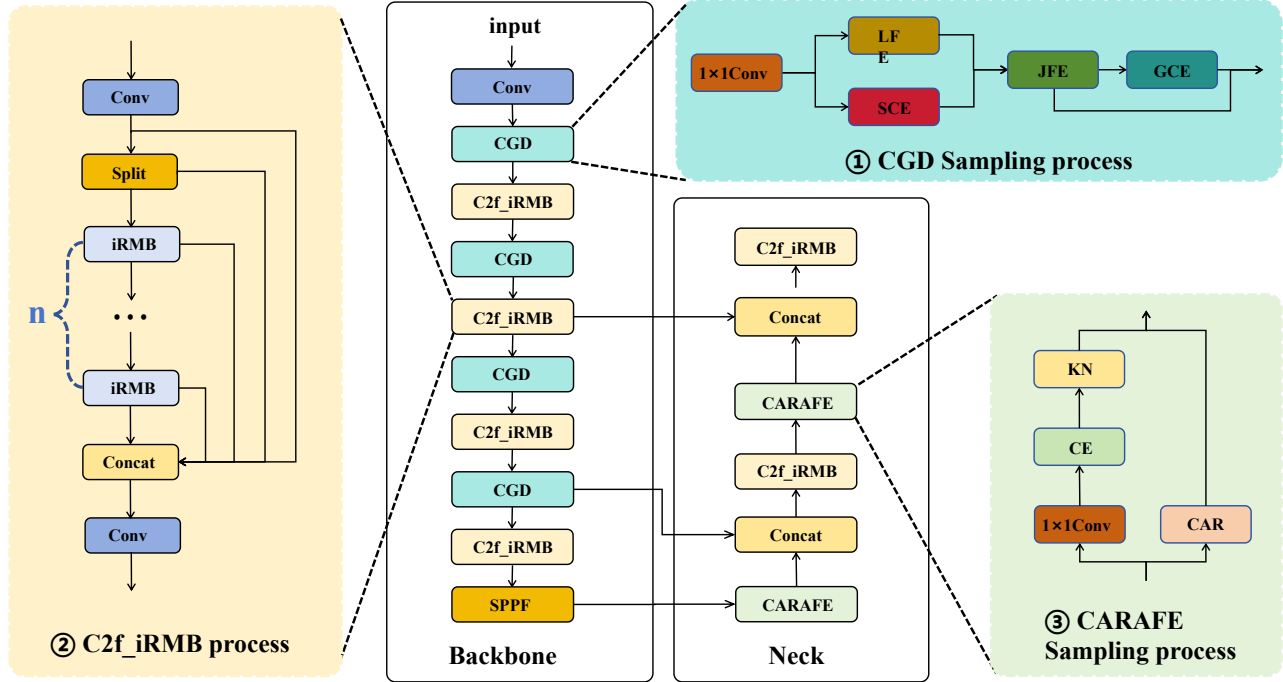


Fig. 2. Illustrates the modifications made to YOLOv8n: in the Backbone section, the original down-sampling convolutional layer was replaced with the CGD down-sampling module, as shown in part ①. In the Neck section, the original Upsample layer was replaced by the CARAFE module, corresponding to part ②. Moreover, the C2f layers in both sections were enhanced by integrating the iRMB module, leading to the new C2f iRMB layer, where n indicates the number of iRMB modules that can be used, as shown in part ③.

ing overall model performance in object detection tasks. The model provides a universal solution with improved real-time performance, data retention, and minimal computational load. The Web-Fire dataset, which we developed, contains fire and smoke instances from both urban and wild settings, and is complemented by the D-Fire dataset [6], covering complex fire scenes. By incorporating novel sampling algorithms and an iRMB to enhance the original C2f, our model addresses high false detection and missed detection rates, along with improved bounding box accuracy in diverse fire and smoke scenarios.

The main contributions of this paper are as follows:

- This paper introduces the CARAFE up-sampling operator and the Context Guided down-sampling module to optimize information retention during the sampling process, ensuring a more comprehensive understanding of contextual content to facilitate the complete transmission of features.
- This paper utilizes the iRMB module to enhance the detection of small targets and smoke. This improves the multi-scale feature extraction capability of the original C2f module. To ensure speed, this paper integrates depthwise convolution and re-evaluates the lightweight CNN architecture from the perspective of efficient unification of IRB and Transformer components. We extend the CNN-based IRB

to an attention-based model and abstract a single residual Meta Mobile Block (MMB) for lightweight model design, balancing parameters while achieving superior detection performance over comparable attention-based models.

II. RELATED WORK

A. Sample

In object detection [27–29], sampling primarily serves to balance the class distribution by selecting positive and negative samples effectively, thereby enhancing model accuracy and training efficiency. Imbalances between positive and negative samples can degrade performance, making sampling strategies essential for optimizing detection capabilities. Effective sampling allows models to focus on critical samples for accurate classification and localization. Dysample [7] introduces an ultra-lightweight, dynamic upsampler that is resource-efficient and easily implemented in PyTorch. Building on this, MFDS-DETR [8] introduces HS-FPN, which further evolves into HSPAN. Downsampling, a common technique for reducing spatial dimensions, is refined with SPD-Conv [9], a new CNN block replacing strided convolution and pooling layers. YOLOv9 [10] presents “adown,” a lightweight downsampling approach that optimizes detection accuracy and efficiency. Each method uniquely improves feature retention during sampling. In contrast, this paper introduces the CARAFE [11]

and CGD [12] modules, which enhance model accuracy by capturing contextual features. Comparative experiments will further demonstrate the effectiveness of these proposed sampling improvements.

B. Transformer

In object detection, Transformers play a critical role in enhancing feature extraction and information aggregation via a powerful self-attention mechanism. This architecture effectively captures global dependencies among objects, thus improving detection accuracy. Unlike traditional Convolutional Neural Networks (CNNs) [13–15], Transformers model relationships across the entire feature map, enabling a more comprehensive representation of object features. Furthermore, Transformers reduce the reliance on anchor boxes and simplify network design, contributing to a more efficient and adaptable detection pipeline. Initially, object detection relied heavily on CNNs for feature extraction and localization. However, in 2020, the introduction of DETR (Detection Transformer) [16] marked a significant shift, bringing Transformers into object detection with an end-to-end approach that simplifies complex anchor and post-processing steps. DETR demonstrated the Transformer’s strengths in modeling long-range dependencies and integrating global features, proving highly effective in complex scenes.

Following DETR, models like Deformable DETR [17] addressed DETR’s slow training and convergence by incorporating a deformable attention mechanism, significantly boosting detection speed and accuracy. Additionally, models such as Swin Transformer [18] combine convolution and Transformer advantages, capturing multi-scale features and improving performance on small objects and complex backgrounds. However, like larger CNNs, Transformers increase model parameters, which can slow down detection. To address this, we introduce the iRMB [19], combining CNN and Transformer elements to improve the C2f module in the original network. This approach leverages both architectures while maintaining detection speed.

III. PROPOSED METHOD

A. Overview

To address the high rates of false negatives and false positives in YOLOv8n[20] for fire detection tasks, this paper introduces CARAFE and CGD sampling modules into the Backbone and Neck sections of the original model. Additionally, the existing C2f modules in both sections were enhanced by incorporating iRMB, resulting in the new C2f_iRMB layer. The improved Backbone and Neck structures as shown in Fig. 2.

B. Content-aware Reassembly of Features Up-sampling Module

The CARAFE module consists of two steps. The first step predicts the reassembly kernel based on the content at each target position, and the second step uses the predicted kernel to reassemble features. Kernel Prediction first reduces

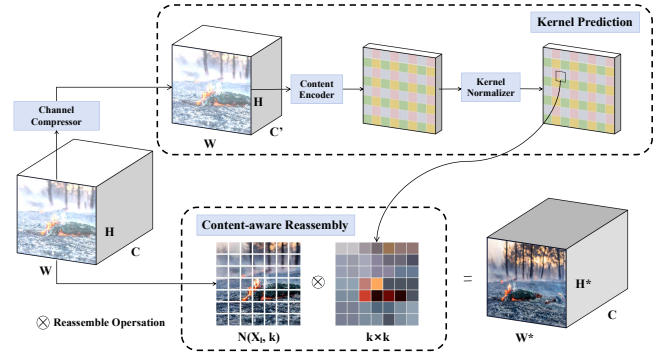


Fig. 3. The overall framework of CARAFE, CARAFE is composed of two key components, .e., kernel prediction module and content-aware reassembly module. A feature map with size $C \times H \times W$ is upsampled by a factor of $a(=2)$ in this figure.

the input channels through a 1×1 convolution to minimize computational cost, followed by a $k \times k$ convolution layer to predict an enlarged up-sampling kernel, representing a larger receptive field. The Content Encoder acts as a $k \times k$ up-sampling kernel. Finally, SoftMax is used to normalize the predicted up-sampling result. Content-Aware Reassembly maps the output back to the input and performs a dot product operation between the $k \times k$ area centered around each point and the predicted result to obtain the output feature map. The detailed sampling process of the module is illustrated in Fig. 3. Given a feature map X of size $H \times W$, the up-sampling process produces a new feature map X^* of size $H^* \times W^*$. For any target position $l' = (i', j')$ in the output X , there exists a corresponding source position $l = (i, j)$ in the input X . Here, $N(X_l, k)$ represents the $N(X_l, k)$ sub-region centered on position l in X . In the first step, the kernel prediction module W predicts the kernel X_l for each position l' based on the neighbors of X_l , as shown in Eq.(1). The reassembly step is formalized in Eq.(2), where φ represents the content-aware reassembly module, which reassembles the neighboring parts of X_l with the kernel W_l .

$$W_l = \psi(N(X_l, k_{encoder})). \quad (1)$$

$$X_l = \phi(N(X_l, k), W_l). \quad (2)$$

The introduction of the CARAFE module helps the model to retain more complete feature information in the Neck section, thereby improving the accuracy of bounding box predictions.

C. Context Guided Down-sampling Module

The CGD module operates by first compressing the input through a 1×1 convolution. This is followed by the Local Feature Extractor (LFE), which uses standard convolution layers to learn local features, and the Surrounding Context Extractor (SCE), which utilizes dilated convolution to capture larger receptive field context. The Joint Feature Extractor (JFE) then fuses local features with surrounding context using Batch

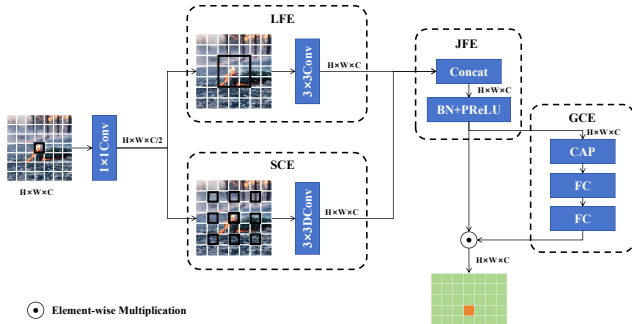


Fig. 4. An overview of the Context Guided Down-sampling Module. The structure of Context Guided block, which consists of local feature extractor LFE, surrounding context extractor SCE, joint feature extractor JFE global context extractor GCE.

Normalization (BN) and ReLU operations. The Global Context Extractor (GCE) performs global average pooling to aggregate the context, followed by two fully connected (FC) layers to weight the features, enhancing the useful parts while suppressing the irrelevant parts. The detailed sampling process of the CGD module is illustrated in Fig. 4. The LFE is specifically designed to learn local features from the input data, using a 3×3 convolutional layer to extract features from local areas of the image. These local features are then combined with surrounding context features, enabling the network to have a comprehensive understanding of different regions. The LFE and SCE work together to ensure that the model not only understands the information of each pixel or local area but also understands the relationships between these areas in the overall context. This detail and local variation overview information is crucial for accurately classifying each pixel in the image, especially for tasks requiring fine-grained predictions, such as distinguishing different objects and surfaces in complex scenes. The use of channel-wise convolutions in LFE and SCE helps reduce cross-channel computational costs, significantly saving memory. This design allows CGD to operate efficiently even in resource-limited environments while maintaining high accuracy and real-time performance.

The SCE increases the receptive field by using dilated convolutions, enabling the model to observe a larger region rather than just focusing on local details. By combining LFE, additional information is provided, helping the model better understand complex scenes. Experiments involving different architectures show that incorporating SCE significantly improves segmentation accuracy.

The role of JFE is to integrate features extracted by LFE and SCE, capturing both local details and broader contextual information. JFE allows the network to consider both local and contextual information, thereby enhancing the accuracy of semantic segmentation. Joint features generated by JFE are further combined with global context features, leveraging information from the entire input image for feature optimization.

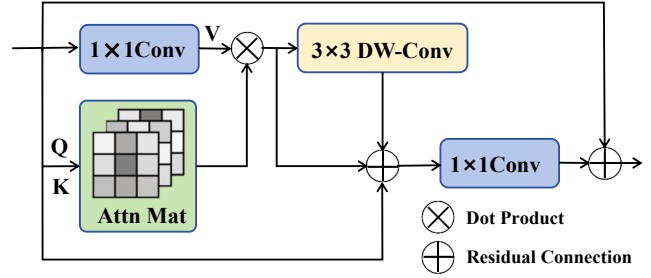


Fig. 5. The iRMB module first extracts value (V) features through a 1×1 convolution, followed by generating the attention matrix (Attn Mat) using query (Q) and key (K). The attention matrix is then multiplied with the value features, and the weighted features are processed by a 3×3 depth-wise convolution (DW-Conv), then added to the input. Subsequently, another 1×1 convolution is applied to integrate the features, and finally, the result is added to the input again to produce the output.

tion. JFE serves as the key connection point that enables the context-guided network to achieve efficient semantic segmentation by balancing local detail and global context.

The GCE captures and leverages global information from the entire input image to enhance the features learned by the joint feature extractor. GCE produces a global feature vector through global average pooling, which captures the average response for each channel in the input image. The global feature vector is then further processed by a multi-layer perceptron (MLP), which learns complex nonlinear relationships between features to refine the global context features. The extracted global context is combined with the joint features via a scale layer, which adjusts the joint features at the channel level, emphasizing the useful features and suppressing the unimportant ones. GCE is an adaptive process because the extracted global context is generated based on the input image, allowing the network to generate customized global context for different images. The introduction of the CGD module helps the model better integrate different local features within the target, enabling more complete feature transmission and reducing the false detection rate while improving the model's testing accuracy.

D. Inverted Residual Mobile block Module

The original bottleneck block had limited multi-scale feature extraction capabilities, but adding multi-head attention mechanisms alone would significantly increase the model's computational cost. Therefore, this paper proposes replacing the bottleneck block in C2f with the Inverted Residual Mobile Block (iRMB) to enhance efficiency and performance on mobile and edge devices. The iRMB combines Depth-Wise Convolution (DW-Conv) and Expanded Window Multi-Head Self-Attention (EW-MHSA) to effectively balance local and global feature extraction, as illustrated in Fig. 5. Specifically, the iRMB consists of the following key components:

1. Depth-Wise Convolution (DW-Conv): DW-Conv is used to efficiently extract spatial features with low computational

TABLE I
COMPARISONS ON WEB-FIRE AND D-FIRE.

Summary		Web-Fire						D-Fire			
ID	Method	Params(M)	Flops(G)	Precision(%)	Recall(%)	mAP50(%)	mAP50:95(%)	Precision(%)	Recall(%)	mAP50(%)	mAP50:95(%)
A	SSD[30]	34.3	31.4	48.6	38.9	36.4	12.5	57.9	52.0	51.7	20.5
B	FCOS[31]	32.2	184	66.6	65.9	67.3	32.9	68.6	63.5	65.2	29.7
C	Faster-R-CNN[32]	33.8	130	61.7	61.7	61.2	27.5	64.3	56.3	58.8	24.7
D	Retinanet[34]	36.5	210	69.0	63.9	66.3	32.8	72.8	63.6	69.7	33.1
E	YOLOv5s[35]	7.0	16.0	66.9	65.5	66.9	33.7	78.2	71.4	76.7	43.0
F	YOLOv7-tiny[36]	6.01	13.1	65.7	66.9	68.0	32.7	75.4	70.2	76.3	40.6
G	YOLOv8n	3.2	8.2	63.6	68.7	68.4	38.2	79.3	69.6	75.4	43.3
H	CCi-YOLOv8n(Ours)	3.8	8.4	69.2	68.8	72.0	41.0	79.5	71.5	78.5	46.6

complexity. DW-Conv operates on each channel individually, significantly reducing the number of parameters and computation. Its computation is defined by Eq.(3).

$$X_{dw} = DW - Conv(X). \quad (3)$$

Where X is the input feature map, and X' is the feature map obtained through depth-wise convolution. 2. Expanded Window Multi-Head Self-Attention (EW-MHSA): EW-MHSA performs multi-head self-attention computation within a local window, reducing the computational cost of traditional self-attention mechanisms. The process is described by Eq.(4),Eq.(5)and Eq.(6).

$$Q = K = X. \quad (4)$$

$$V = Expand(X). \quad (5)$$

$$Attention(Q, K, V) = soft \max\left(\frac{QK^T}{\sqrt{d_k}}\right)V. \quad (6)$$

where Q,K and V represent query, key, and value, respectively, and Expand represents the channel extension operation.

3. Feed-Forward Network (FFN): After EW-MHSA, the feature map is further transformed by the feed-forward network, consisting of two linear layers and a nonlinear activation function. Its computation is represented by Eq.(7).

$$X_{ffn} = FFN(X_{att}). \quad (7)$$

4. Residual Connections: To facilitate efficient gradient flow and avoid gradient vanishing, residual connections are added to iRMB. These connections ensure that the output retains input information, assisting in training deeper networks. The final output is obtained through residual connections, as shown in Eq.(8).

$$Y = X + X_{ffn}. \quad (8)$$

By combining DW-Conv and EW-MHSA, iRMB achieves a good balance between capturing local and global features. The attention mechanism within the local window reduces the quadratic complexity of the traditional self-attention mechanism, making this design more feasible for practical applications. Improving the original C2f module using this block enhances the model's ability to detect small targets and reduces the missed detection rate.

IV. EXPERIMENT AND ANALYSIS

The experimental setup of this study includes the following: CPU: INTEL-XEON 6230, GPU: NVIDIA GeForce RTX 4090, system environment: Ubuntu 22.04, programming language: Python 3.9, accelerated environment: CUDA 12.2, PyTorch version: 2.0.0. The datasets used in the experiment include a custom fire dataset named "Web-Fire" and an open dataset named "D-Fire."

A. Datasets

Web-Fire The custom fire dataset contains 11,646 images, divided into 10,481 training images and 1,165 test images with a ratio of 9:1, ensuring the complexity and completeness of the dataset, allowing the model to accurately detect various fire scenarios.

D-Fire The D-Fire dataset, developed by Gaia researchers, is a specialized image dataset for fire and smoke detection, containing over 21,000 images divided into four categories: fire only (1,164 images), smoke only (5,867 images), both fire and smoke (4,658 images), and neither fire nor smoke (9,838 images).

B. Evaluation Metrics

The evaluation indicators for experiments in this paper include Precision, Recall, and mAP. where precision is how many of the samples that the model predicts to be positive are correct, and recall is how many of the samples that are truly positive are correctly predicted to be positive. mAP is further divided into mAP50 and mAP50-0.95, which represent the average accuracy of IoU between 0.5 and 0.5-0.95, respectively.

C. Comparison with State-of-the-art Methods

Table I present a comparison between CCi-YOLOv8n and other models on the Web-Fire and D-Fire datasets. In addition to the four indicators mentioned earlier, parameter and Flops are also introduced to better reflect the comparison between models. The results demonstrate that the CCi-YOLOv8n model significantly outperforms others in terms of target detection performance, achieving the highest scores for mAP50 and mAP50-0.95. Specifically, CCi-YOLOv8n attained 72.0%

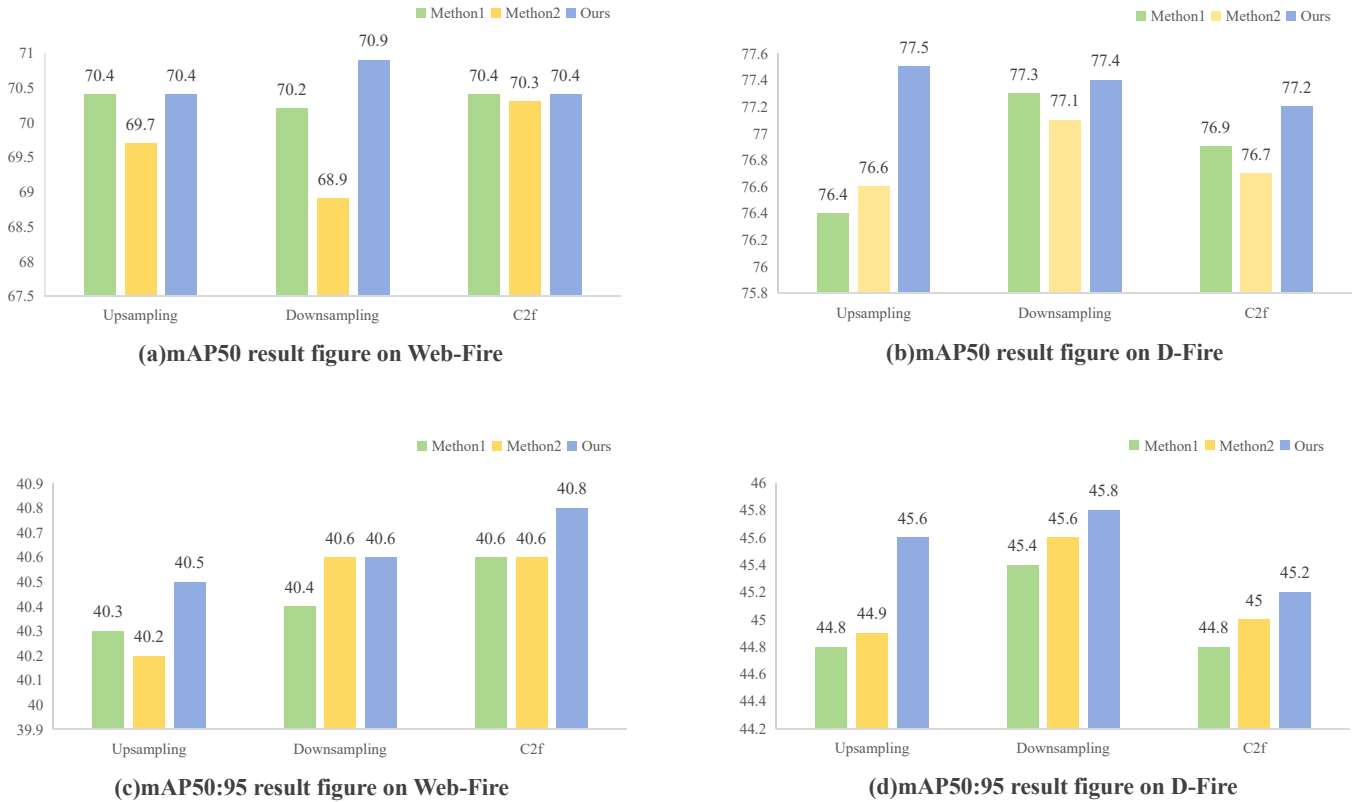


Fig. 6. Method1 of the upsampling part is dysample, and method2 is HSPAN. Method1 of the downsampling part is adown, and method2 is SPDCConv. Method1 of the c2f part is RVB[21], and method2 is PKI[22]. The modules used in this paper have good performance in each part.

TABLE II
THE RESULTS(%) ABLATION TESTS ON WEB-FIRE AND D-FIRE.

Summary	Web-Fire							D-Fire				
	ID	CARAFE	CGD	iRMB	Precision	Recall	mAP50	mAP50:95	Precision	Recall	mAP50	mAP50:95
1					63.4	68.7	68.4	38.4	79.3	69.6	75.4	43.3
2		✓			69.0	65.8	70.3	40.0	79.0	71.1	77.8	45.9
3		✓	✓		69.1	68.8	70.9	40.0	78.6	71.7	78.2	46.4
4		✓	✓	✓	69.2	68.8	72.0	41.0	79.5	71.7	78.5	46.6

and 41.0% for the two metrics on the Web-Fire dataset, and 78.5% and 46.6% on the D-Fire dataset. We added a small amount of computation based on the original model, but our model performed well on other indicators. Additionally, CCI-YOLOv8n has fewer parameters and FLOPs, achieving a substantial reduction in computational requirements compared to earlier models while maintaining high precision.

D. Ablation Studies and Analysis

The comparison results presented in Fig 6, demonstrate that the proposed CCI-YOLOv8n method is superior to many state-of-the-art object detection methods. In what follows, the proposed CCI-YOLOv8n method is comprehensively analyzed from three aspects to investigate the logic behind its superiority. (1) Role of CARAFE upsampling. Compared with other

upsampling modules including dysample and HSPAN, ours performs the best in both mAP50 and mAP50:95 metrics on the web fire dataset and dfire dataset. (2) Influence of CGD downsampling. In terms of performance in the downsampling section, our module has also shown the best performance along with Adown and SPDCConv. (3) Impact of iRMB-C2f. Our module has been compared with recently proposed PKI and RVB methods and has shown the best performance.

The experimental results indicate that when CARAFE and CGD modules were introduced individually, significant improvements in precision and mAP were observed, especially in mAP50. When both CARAFE and CGD were introduced together, the model's overall performance was optimal, particularly in terms of mAP50-0.95, demonstrating the synergy between CARAFE and CGD modules, which not only im-

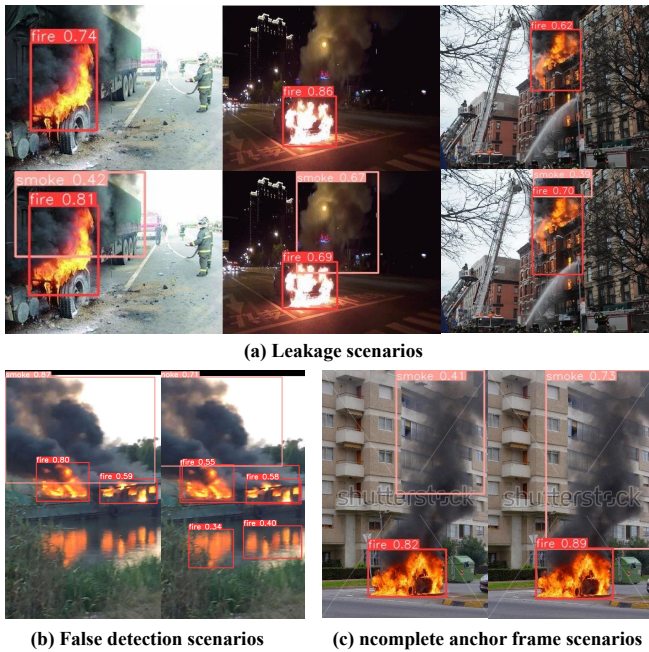


Fig. 7. A visual comparison of the original model with our model in three scenarios.

proved performance at a single threshold but also enhanced average precision across different threshold ranges, thus improving the overall detection capability and robustness of the model. Therefore, the comprehensive use of these two modules can significantly enhance the performance of the fire and smoke detection system, providing more accurate and reliable results, the results as shown in Table II.

E. Visualization

To visually demonstrate the effectiveness of the improved model, examples of detection on problematic data from the original model were selected, as shown in Fig. 6. (a) shows cases of missed detection; (b) illustrates false detection cases, and (c) demonstrates incomplete bounding boxes. The experiments indicate that the improved model not only detects targets that were previously undetected by the original model but also reduces the false detection rate and provides more complete target detection, validating the advancement of the improved model with increased overall accuracy.

V. CONCLUSION

In this study, a fire dataset named "Web-Fire" was proposed, alongside an improved model, CCI-YOLOv8n, built upon YOLOv8n. Extensive experiments were conducted on both the custom-made Web-Fire dataset and the publicly available D-Fire dataset. The results demonstrated that the improved model enhances accuracy while incurring minimal additional computational overhead. The proposed model showed varying performances across different datasets, highlighting its versatility. Future work will focus on further improving the

model's generalizability and computational speed to expand its practical applicability.

REFERENCES

- [1] F. M. Talaat and H. ZainEldin, "An improved fire detection approach based on yolo-v8 for smart cities," *Neural Computing and Applications*, vol. 35, pp. 20 939–20 954, 2023.
- [2] G. N. Rao, P. J. Rao, R. Duvvuru, K. Beulah, E. L. Lydia, P. Rathnala, B. Balakrishna, and V. R. Motru, "Neural fuzzy system design in forest fire detection," *Microsystem Technologies*, vol. 30, pp. 455–467, 2024.
- [3] A. S. Almasoud, "Intelligent deep learning enabled wild forest fire detection system," *Computer Systems Science and Engineering*.
- [4] Z. Hong, Z. Tang, H. Pan, Y. Zhang, Z. Zheng, R. Zhou, Z. Ma, Y. Zhang, Y. Han, J. Wang, and S. Yang, "Active fire detection using a novel convolutional neural network based on himawari-8 satellite images," in *Frontiers in Environmental Science*, 2022.
- [5] H. Zheng, J. Duan, Y. Dong, and Y. Liu, "Real-time fire detection algorithms running on small embedded devices based on mobilenetv3 and yolov4," *Fire Ecology*, vol. 19, pp. 31–, 2023.
- [6] de Venâncio, P. V. A. B., L. A. C., and B. A. V., "An automatic fire detection system based on deep convolutional neural networks for low-power, resource-constrained devices," *Neural Computing and Applications*, vol. 34, pp. 15 349–15 368, 2022.
- [7] W. Liu, H. Lu, H. Fu, and Z. Cao, "Learning to upsample by learning to sample," in *2023 IEEE/CVF International Conference on Computer Vision (ICCV)*, 2023, pp. 6004–6014.
- [8] R. Sunkara and T. Luo, "No more strided convolutions or pooling: A new cnn building block for low-resolution images and small objects," in *ECML/PKDD*, 2022.
- [9] Y. Chen, C. Zhang, B. Chen, Y. Huang, Y. Sun, C. Wang, X. Fu, Y. Dai, F. Qin, Y. Peng, and Y. Gao, "Accurate leukocyte detection based on deformable-detr and multi-level feature fusion for aiding diagnosis of blood diseases," *Computers in Biology and Medicine*, vol. 170, p. 107917, 2024.
- [10] C.-Y. Wang, I.-H. Yeh, and H. Liao, "Yolov9: Learning what you want to learn using programmable gradient information," *ArXiv*, vol. abs/2402.13616, 2024.
- [11] J. Wang, K. Chen, R. Xu, Z. Liu, C. C. Loy, and D. Lin, "Carafe: Content-aware reassembly of features," in *2019 IEEE/CVF International Conference on Computer Vision (ICCV)*, 2019, pp. 3007–3016.
- [12] T. Wu, S. Tang, R. Zhang, and Y. Zhang, "Cgnet: A lightweight context guided network for semantic segmentation," *IEEE Transactions on Image Processing*, vol. 30, pp. 1169–1179, 2018.
- [13] F. Shen, X. Shu, X. Du, and J. Tang, "Pedestrian-specific bipartite-aware similarity learning for text-based person

- retrieval,” in *Proceedings of the 31th ACM International Conference on Multimedia*, 2023.
- [14] F. Shen, X. Du, L. Zhang, and J. Tang, “Triplet contrastive learning for unsupervised vehicle re-identification,” *arXiv preprint arXiv:2301.09498*, 2023.
- [15] Y. Lecun, L. Bottou, Y. Bengio, and P. Haffner, “Gradient-based learning applied to document recognition,” *Proceedings of the IEEE*, vol. 86, no. 11, pp. 2278–2324, 1998.
- [16] N. Carion, F. Massa, G. Synnaeve, N. Usunier, A. Kirillov, and S. Zagoruyko, “End-to-end object detection with transformers,” *ArXiv*, vol. abs/2005.12872, 2020.
- [17] X. Zhu, W. Su, L. Lu, B. Li, X. Wang, and J. Dai, “Deformable detr: Deformable transformers for end-to-end object detection,” *ArXiv*, vol. abs/2010.04159, 2020.
- [18] Y. Xie, X. Ma, and Q. Zhao, “Research on target detection network based on improved swin-detr,” in *2023 4th International Conference on Big Data, Artificial Intelligence and Internet of Things Engineering (ICBAIE)*, 2023, pp. 324–328.
- [19] J. Zhang, X. Li, J. Li, L. Liu, Z. Xue, B. Zhang, Z. Jiang, T. Huang, Y. Wang, and C. Wang, “Rethinking mobile block for efficient attention-based models,” in *Proceedings of the IEEE/CVF International Conference on Computer Vision (ICCV)*, October 2023, pp. 1389–1400.
- [20] G. Jocher, J. Qiu, and A. Chaurasia, “Ultralytics YOLO,” Jan. 2023.
- [21] A. Wang, H. Chen, Z. Lin, H. Pu, and G. Ding, “Rep vit: Revisiting mobile cnn from vit perspective,” *2024 IEEE/CVF Conference on Computer Vision and Pattern Recognition (CVPR)*, pp. 15 909–15 920, 2023.
- [22] X. Cai, Q. Lai, Y. Wang, W. Wang, Z. Sun, and Y. Yao, “Poly kernel inception network for remote sensing detection,” *2024 IEEE/CVF Conference on Computer Vision and Pattern Recognition (CVPR)*, pp. 27 706–27 716, 2024.
- [23] W. Weng, M. Wei, J. Ren, and F. Shen, “Enhancing aerial object detection with selective frequency interaction network,” *IEEE Transactions on Artificial Intelligence*, vol. 1, no. 01, pp. 1–12, 2024.
- [24] H. Li, R. Zhang, Y. Pan, J. Ren, and F. Shen, “Lr-fpn: Enhancing remote sensing object detection with location refined feature pyramid network,” *arXiv preprint arXiv:2404.01614*, 2024.
- [25] C. Qiao, F. Shen, X. Wang, R. Wang, F. Cao, S. Zhao, and C. Li, “A novel multi-frequency coordinated module for sar ship detection,” in *2022 IEEE 34th International Conference on Tools with Artificial Intelligence (ICTAI)*. IEEE, 2022, pp. 804–811.
- [26] W. Weng, W. Lin, F. Lin, J. Ren, and F. Shen, “A novel cross frequency-domain interaction learning for aerial oriented object detection,” in *Chinese Conference on Pattern Recognition and Computer Vision (PRCV)*. Springer, 2023, pp. 292–305.
- [27] K. Yan, F. Shen, and Z. Li, “Enhancing landslide segmentation with guide attention mechanism and fast fourier transformer,” in *International Conference on Intelligent Computing*. Springer, 2024, pp. 296–307.
- [28] Y. Tang, H. Pan, J. Guo, F. Shen, Z. Zhu, and H. Jia, “Fourier-fpn: Fourier improves multi-scale feature learning for oriented tiny object detection,” in *International Conference on Intelligent Computing*. Springer, 2024, pp. 450–461.
- [29] C. Liu, X. Qi, H. Yin, B. Song, K. Li, and F. Shen, “Feature pyramid full granularity attention network for object detection in remote sensing imagery,” in *International Conference on Intelligent Computing*. Springer, 2024, pp. 332–353.
- [30] W. Liu, D. Anguelov, D. Erhan, C. Szegedy, S. Reed, C.-Y. Fu, and A. C. Berg, “Ssd: Single shot multibox detector,” in *Computer Vision – ECCV 2016*, B. Leibe, J. Matas, N. Sebe, and M. Welling, Eds. Cham: Springer International Publishing, 2016, pp. 21–37.
- [31] Z. Tian, C. Shen, H. Chen, and T. He, “Fcos: Fully convolutional one-stage object detection,” in *2019 IEEE/CVF International Conference on Computer Vision (ICCV)*, 2019, pp. 9626–9635.
- [32] S. Ren, K. He, R. Girshick, and J. Sun, “Faster r-cnn: Towards real-time object detection with region proposal networks,” *IEEE Transactions on Pattern Analysis and Machine Intelligence*, vol. 39, no. 6, pp. 1137–1149, 2017.
- [33] Z. Cai and N. Vasconcelos, “Cascade r-cnn: High quality object detection and instance segmentation,” *IEEE Transactions on Pattern Analysis and Machine Intelligence*, vol. 43, no. 5, pp. 1483–1498, 2021.
- [34] T.-Y. Lin, P. Goyal, R. Girshick, K. He, and P. Dollár, “Focal loss for dense object detection,” in *2017 IEEE International Conference on Computer Vision (ICCV)*, 2017, pp. 2999–3007.
- [35] G. Jocher, “YOLOv5 by Ultralytics,” May 2020.
- [36] C.-Y. Wang, A. Bochkovskiy, and H.-Y. M. Liao, “Yolov7: Trainable bag-of-freebies sets new state-of-the-art for real-time object detectors,” in *2023 IEEE/CVF Conference on Computer Vision and Pattern Recognition (CVPR)*, 2023, pp. 7464–7475.